

Simulating Quantum Walk Hamiltonians without Pauli Decomposition

Mostafa Atallah^{1,3}, Alvin Gonzales², Daniel Dilley², Igor Gaidai^{1,4}, Zain H. Saleem², and Rebekah Herrman¹^{*}

¹*Department of Industrial and Systems Engineering, University of Tennessee Knoxville, USA*

²*Mathematics and Computer Science Division, Argonne National Laboratory, Lemont, IL, USA*

³*Department of Physics, Faculty of Science, Cairo University, Giza 12613, Egypt*

⁴*Department of Physics and Astronomy, University of Tennessee Chattanooga, USA*

(Dated: January 19, 2026)

In this work, we present a new algorithm for generating quantum circuits that efficiently implement continuous time quantum walks on arbitrary simple sparse graphs. The algorithm, called matching decomposition, works by decomposing a continuous-time quantum walk Hamiltonian into a collection of exactly implementable Hamiltonians corresponding to matchings in the underlying graph followed by a novel graph compression algorithm that merges edges in the graph. Lastly, we convert the walks to a circuit and Trotterize over these components. The dynamics of the walker on each edge in the matching can be implemented in the circuit model as sequences of CX and CRx gates. We do not use Pauli decomposition when implementing walks along each matching. Furthermore, we compare matching decomposition to a standard Pauli-based simulation pipeline and find that matching decomposition consistently yields substantial resource reductions, requiring up to 43% fewer controlled gates and up to 54% shallower circuits than Pauli decomposition across multiple graph families. Finally, we also present examples and theoretical results for when matching decomposition can exactly simulate a continuous-time quantum walk on a graph.

I. INTRODUCTION

Hamiltonian simulation is a central primitive in quantum computing, and a wide variety of techniques have been developed for it. Some Hamiltonian simulation approaches rely on structured access to the Hamiltonian, for example through oracles [1–3], compressed quantum states [4], or block encodings [5]. Other techniques excel on particular kinds of Hamiltonians such as sparse Hamiltonians [6] or Hamiltonians where the underlying problem has some symmetry [7].

A Continuous-Time Quantum Walk (CTQW) is a quantum process whose dynamics can be described by e^{-iAt} where a Hamiltonian A is an adjacency matrix of some unweighted graph and t is the propagation time. Thus, we can equivalently say that CTQW is a process driven by a given graph.

CTQWs are known to form a universal model of quantum computation [8–10] and have a wide range of applications, including spatial search [11–14], link prediction [15, 16], quantum simulation [17], optimization [18, 19], variational quantum algorithms [20], quantum state preparation [21], biological processes [22, 23], and more [24, 25]. Although CTQWs can be implemented using waveguides [26, 27] or photonic chips [7, 28, 29], only CTQWs on specific classes of graphs, such as circulant graphs, stars, and graph products, can be exactly implemented in the circuit model [7, 30–34]. CTQWs on other classes of graphs can be approximated by decomposing the adjacency matrix (or Laplacian) of the underlying graph into smaller matrices and Trotterizing over the smaller matrices [35, 36].

CTQWs on dynamic graphs provide a more direct bridge to the standard circuit model [10]. In this framework, computation is performed by evolving under a time-ordered sequence of adjacency matrices, and the resulting dynamics constitute a universal model of quantum computation [10]. Subsequent work has extended this framework in several directions, including the addition of isolated vertices [37], simplification techniques [38], methods to write an arbitrary gate in terms of at most three graphs [39], and a detailed characterization of the relationship between CTQWs on dynamic graphs and the multi-angle quantum approximate optimization algorithm (MA-QAOA) [40], which connects CTQWs on dynamic graphs to the broader context of QAOA-like variational algorithms [41–44].

More recently, CTQWs on dynamic graphs were used to implement a sparse state preparation circuit using $O(nm)$ CX gates, where n is the number of qubits and m is the number of nonzero amplitudes in the target state [21]. The work relies on converting single edges and self-loops in the dynamic graph framework to sequences of CRx, CP, and CX gates, thus motivating the idea that arbitrary CTQWs can be simulated in the circuit model using similar decomposition approaches. The authors show that these sequences can generate any unitary [21]. Related quantum-walk-based state preparation schemes have also been proposed in other settings, for example, to prepare angular momentum eigenstates [45]. Other decomposition-based approaches include decomposing graphs into star subgraphs and performing Trotterization over the stars [46] and decomposing the Laplacian of a graph into smaller pieces to use for Trotterization [36].

Another variation of CTQW is a CTQW on *state space*, where the graph corresponding to the walk is defined di-

* corresponding author; rherrma2@utk.edu

rectly on a state space. The key difference is that in this formulation we are required to respect a particular embedding of the graph into the state space when simulating the walk, which is important when CTQW is used as an intermediate building block of a quantum circuit. Note that, given an unlabeled graph, one can label the vertices of the graph in order to perform a CTQW on a state space.

In general, implementing an arbitrary CTQW requires exponentially many quantum gates and classical computational resources in the number of qubits. However, a sparse CTQW, that is a CTQW where the number of edges grows polynomially in the number of qubits, can be implemented using fewer resources.

In this work, we develop an algorithm that generates a quantum circuit for a given sparse CTQW on state space. Our algorithm is based on decomposition of CTQW edges into a collection of matchings. A novel graph compression algorithm is used to combine edges, which reduces CX gate overhead in the output circuit. The overall evolution can then be approximated via Trotterization over the set of matchings [47]. As with any Trotterization methods, the approximation error can be arbitrarily reduced by increasing the number of Trotter steps.

In our numerical benchmarks we compare against a standard Pauli decomposition Trotterization workflow with identical transpilation settings. We emphasize that Pauli-based Hamiltonian simulation is a mature direction, and a number of specialized Pauli evolution compilation techniques (e.g., cancellation-aware synthesis and dedicated Pauli compilers) can further reduce two-qubit gate counts [48]. Our goal here is to evaluate whether matching decomposition provides a new circuit construction primitive that is competitive against a widely used baseline, and to quantify the practical gains that can be obtained immediately in a standard toolchain.

In Sec. II, we present a formal definition for a CTQW on a dynamic graph sequence and define the basic graph theory terminology used in this work. In Sec. III, we describe the matching decomposition algorithms. In Sec. IV, we compare the 2-norm of the operator difference between the exact CTQW time evolution operator and the matching decomposition, as well as Pauli decomposition [49] and find that the two decompositions have comparable accuracy. We also find that the matching decomposition approach requires up to 43% fewer CX gates and up to 54% shallower circuits than Pauli decomposition when using both methods to approximate CTQWs on select graphs. We also analyze when a given graph has a matching decomposition that pairwise commute. In Sec. V, we discuss the implications of our findings and potential future directions.

II. BACKGROUND

In this section, we give a brief introduction to continuous-time quantum walks on dynamic graphs,

graph theory terminology, Trotterization, and Pauli decomposition.

A. Continuous-time quantum walks on dynamic graphs

A *continuous-time quantum walk on a dynamic graph*, $G = \{(G_i, t_i)\}_{i \in [m]}$ is defined by an ordered sequence of graphs G_i and associated propagation times t_i . A walker traverses each graph for the associated time according to

$$|\psi_f\rangle = e^{-iA_m t_m} \dots e^{-iA_1 t_1} |\psi_0\rangle$$

where $|\psi_0\rangle$ is the initial state of the walker and A_i is the adjacency matrix of graph G_i .

The authors of [21] showed how to map CTQWs on single edge walks and self-loop graphs into the circuit model using CRx, CRz, and CP gates. In this approach, each vertex of the graph is labeled by a bitstring of length n . We make extensive use of the single edge conversion. The single-edge conversion will rely on the *Hamming distance* between two labels. The Hamming distance of two bitstrings u and v is the number of positions in which the two bitstrings differ and is denoted $d_H(u, v)$. Given an edge between two standard basis states z_1 and z_2 that are Hamming distance one apart, the circuit is a multi-controlled Rx gate,

$$\text{Rx}(2t) = \begin{pmatrix} \cos(t) & -i \sin(t) \\ -i \sin(t) & \cos(t) \end{pmatrix}, \quad (1)$$

with a target on the differing qubit and controls matching the other qubits. For z_1 and z_2 greater than Hamming distance one apart, a similar approach can be applied. First, a basis transformation is performed. CX gates are applied such that the control is a fixed qubit where z_1 and z_2 differ and the targets are the remaining differing qubits. This brings z_1 and z_2 to Hamming distance one apart. Second, the multicontrolled Rx gate is applied as before. Finally, the CX gates are applied again to restore the basis.

These circuits were then used to make an efficient sparse deterministic state preparation algorithm that also utilized ideas from classical combinatorics to minimize the controlled gate count. The Hamiltonian simulation algorithm in this paper is inspired by a multi-edge version of the CTQW mapping from [21].

B. Graph theory terminology

Throughout this work, we will focus on *simple* graphs $G = (V, E)$ that have no self-loops or multi-edges. A *matching* of G is defined to be a set of edges $M \subseteq E$ such that no two edges in M share a common vertex. A graph matching is said to be *maximal* if it is not a subset of any other matching of G . A matching M of G is said to be *perfect* if $|M| = |V|/2$. Graph matchings

have applications in fields such as image analysis [50], chemical compound analysis [51], and computer science [52, 53]. Furthermore, there exist several graph matching algorithms and heuristics that can be implemented in polynomial time [54–59]. Note that a graph can have several different matchings, so the matching algorithms used in this paper are not deterministic in general. Thus, there may be some slight differences in circuits when using the Trotterization methods in this work.

A graph is said to be *bipartite* if its vertices can be partitioned into two disjoint sets such that every edge has an endpoint in both sets, or equivalently, the graph contains no cycles of odd length. Two graphs commonly discussed in later sections are complete graphs on 2 vertices (equivalently single edges), denoted K_2 , and cycles with four vertices, denoted C_4 , both of which are examples of bipartite graphs. A *cycle* on n vertices is a connected graph with n vertices where each vertex is incident to exactly two edges. Note that C_n is bipartite if and only if n is even. $K_{n,n}$ is another such bipartite graph mentioned below and is defined as a graph with $2n$ vertices that are partitioned into two sets of size n such that all vertices in one set are connected to all vertices in the other set by edges and no vertices are connected to any vertex in the same set.

C. Trotter Decomposition

An arbitrary Hamiltonian A_G can be decomposed into a set of matrices $\{A_i\}$. Then, by the Trotter-Lie formula [60],

$$\lim_{N \rightarrow \infty} \left(e^{-i \frac{t}{N} A_1} e^{-i \frac{t}{N} A_2} \cdots e^{-i \frac{t}{N} A_m} \right)^N = e^{-itA_G} \quad (2)$$

with error $O(t^2/N)$ for finite N . This approach is commonly used to simulate Hamiltonians on gate-based quantum computers.

III. MATCHING DECOMPOSITION ALGORITHM

In this section, we describe our approach for implementing continuous-time quantum walks (CTQWs) on sparse graphs embedded into a state space in the circuit model. The method consists of two main steps: (1) decomposing a graph into matchings, and (2) applying iterative graph compression on the matchings to minimize the number of control qubits required for circuit implementation.

A. Greedy matching decomposition

Since edges in a matching are independent (i.e., no two edges share a common vertex), time evolution operators

under each edge in the matching commute, and the total matching evolution $e^{-iA_M t}$ can be decomposed into independent single-edge operations. Since the embedding of the graph is fixed, each vertex is labeled with an n -bit string corresponding to a basis state $|z\rangle$.

Our algorithm decomposes the graph edges into matchings by grouping edges according to their *bit-flip structure*. The bit-flip structure of an edge (u, v) is determined by which bit positions differ between the endpoint labels u and v . We first identify edges with Hamming distance $d_H(u, v) = 1$. For such edges, we define the *bit-flip position* as the unique bit index i where u and v differ. For example, the edge $(010, 110)$ has bit-flip position 2, since only the third bit (index 2) differs between the endpoints. Here and further in the text, the bit indices are assigned from right to left and are indexed starting with “0”.

The key insight is that walks along edges sharing the same bit-flip position i all correspond to controlled Rx rotations with target qubit i and different sets of control bits. This makes them natural candidates for grouping into the same matching, as the resulting circuit can potentially be compressed using the graph compression technique described in Section III B.

The greedy matching algorithm (Algorithm 1) partitions edges into matchings as follows: edges with Hamming distance 1 are grouped by their bit-flip position. Crucially, edges with the same bit-flip position cannot share a vertex – if two edges (u_1, v_1) and (u_2, v_2) both flip bit i , then sharing a vertex would imply $u_1 = u_2$ (or some permutation), which forces $v_1 = v_2$ since both flip only bit i . Thus, each bit-flip group is already a valid matching. Edges with Hamming distance greater than one are greedily added to existing matchings if they share no vertices with any edge already in an existing matching in order to reduce the total number of matchings, but they benefit from graph compression in a different way. See Sec. III D for an example of the matching algorithm.

B. Iterative graph compression

After decomposing the graph into matchings, we apply an iterative graph compression technique to each matching in the decomposition. The graph compression combines edges of the graph, which consequently reduces the number of edges and both the number of multicontrolled Rx gates and controls in the multicontrolled Rx gates of the output circuit. Recall from Section II A that each edge (z_1, z_2) in a graph is implemented as a multicontrolled Rx gate: the target qubit is one of the bit positions where z_1 and z_2 differ, and the control qubits are determined by the common bits of z_1 and z_2 . When multiple bit positions differ (i.e., Hamming distance greater than one), we select any one of the differing positions as the target qubit and apply controlled-NOT gates to the other differing positions, as described in Section II A. The goal of graph compression is to merge multiple edges into a single edge in a reduced qubit space, thereby reducing

Algorithm 1: Greedy Matching Decomposition

```

Input: Edge set  $E$  with  $n$ -bit vertex labels
Output: List of matchings  $\mathcal{M} = \{M_1, M_2, \dots\}$ 
// Group edges by bit-flip position
1 for each edge  $(u, v) \in E$  do
2   if  $d_H(u, v) = 1$  then
3      $i \leftarrow$  bit position where  $u$  and  $v$  differ;
4     Add  $(u, v)$  to group  $G_i$ ;
5   else
6     Add  $(u, v)$  to  $E_{\text{multi}}$ ; // Hamming dist > 1
7   end
8 end
9  $\mathcal{M} \leftarrow \emptyset$ ;
// Create matchings from each bit-flip group
10 for each bit position  $i$  with  $G_i \neq \emptyset$  do
11    $\mathcal{M} \leftarrow \mathcal{M} \cup \{G_i\}$ ;
12 end
13 for each edge  $e \in E_{\text{multi}}$  do
14   Place  $e$  in first  $M \in \mathcal{M}$  with no vertex conflict, or
     create new  $M$ ;
15 end
16 return  $\mathcal{M}$ ;

```

the number of control qubits needed.

Let $M = \{e_1, \dots, e_m\}$ be a matching where each edge $e_i = (u_i, v_i)$ connects vertices labeled by n -bit strings $u_i, v_i \in \{0, 1\}^n$. We refer to the graph at iteration zero as G_0 .

To describe the compression algorithm precisely, we introduce several definitions. First, we need a way to identify which bit positions differ between the endpoints of an edge, as this determines the target qubit for the corresponding Rx gate.

Definition 1 (XOR Mask). *For an edge (u, v) with n -bit vertex labels, the XOR mask is $\mu = u \oplus v \in \{0, 1\}^n$, where bit k of μ is 1 if and only if u and v differ at position k . We distinguish between the original XOR mask (computed from the original n -bit labels, which never changes during compression) and the current XOR mask (computed from the current compressed labels).*

As edges are merged, the bit-string labels become shorter. We need to track which original qubit indices remain in the compressed representation.

Definition 2 (Active Qubits). *The active qubits $\mathcal{A} = (a_0, a_1, \dots, a_{m-1})$ is an ordered list of original qubit indices that remain after edge merging. Initially, $\mathcal{A} = (0, 1, \dots, n-1)$. When two edges are merged by removing the bit at position p in the current compressed labels, the corresponding original qubit index a_p is removed from \mathcal{A} . The compressed edge labels are m -bit strings, where $m = |\mathcal{A}|$, and bit position p in the compressed label corresponds to original qubit a_p .*

When a qubit is removed during compression and that qubit corresponded to a differing bit in the original edge (i.e., the original XOR mask has a 1 at that position), we

must track this for circuit construction. These qubits require additional controlled-NOT gates to implement the basis transformation described in Section II A.

Definition 3 (Weight-Reducing Qubits). *The weight-reducing qubits \mathcal{W}_e is an ordered list of original qubit indices that were removed during compression and correspond to differing bits in the original edge. Initially, \mathcal{W}_e is empty. When two edges are merged by removing the bit at position p , if the original qubit index a_p corresponds to a 1 in the original XOR mask μ_e (i.e., bit a_p is set in μ_e), then a_p is appended to \mathcal{W}_e of the merged edge. These qubits are called “weight-reducing” because removing them reduces the Hamming weight of the current XOR mask relative to the original.*

With these concepts in place, we can now define when two edges can be merged into a single edge in a reduced qubit space.

Definition 4 (Mergeable edges). *Two edges $e_1 = (u_1, v_1)$ and $e_2 = (u_2, v_2)$ are mergeable at position p (where p is a position in the current compressed labels) if:*

1. *The edges have equal original XOR masks ($\mu_{e_1} = \mu_{e_2}$),*
2. *The active qubit lists are equal ($\mathcal{A}_{e_1} = \mathcal{A}_{e_2}$),*
3. *The weight-reducing qubit lists are equal ($\mathcal{W}_{e_1} = \mathcal{W}_{e_2}$), and*
4. *The endpoints differ only at position p : either $(u_1 \oplus u_2 = v_1 \oplus v_2 = 2^p)$ or $(u_1 \oplus v_2 = v_1 \oplus u_2 = 2^p)$.*

Note that conditions 1–3 together imply the current XOR masks are also equal. The last condition ensures that after deleting bit p , both edges collapse to the same edge in the reduced space.

The result of merging two edges is a compressed edge with fewer bits in its vertex labels.

Definition 5 (Compressed Edge). *A compressed edge $e' = (u', v') \in \{0, 1\}^m \times \{0, 1\}^m$ is an edge with m -bit vertex labels, where $m \leq n$. Each compressed edge has associated metadata:*

- $\mathcal{A}_{e'} = (a_0, \dots, a_{m-1})$: the ordered list of active original qubit indices, where bit position p in e' corresponds to original qubit a_p ,
- $\mathcal{W}_{e'}:$ the list of weight-reducing original qubit indices (a subset of the deleted qubits), and
- $\mu_{e'} \in \{0, 1\}^n$: the original XOR mask.

A compressed edge represents 2^{n-m} original edges: expanding e' by inserting bits at the deleted qubit positions with all 2^{n-m} combinations yields the original edge set.

Finally, we define the operation that removes a bit from vertex labels when merging two edges.

Definition 6 (Bit Deletion Operator). *The bit deletion operator $\pi_k : \{0, 1\}^n \rightarrow \{0, 1\}^{n-1}$ removes bit k from an n -bit string:*

$$\pi_k(b_{n-1} \cdots b_k \cdots b_0) = b_{n-1} \cdots b_{k+1} b_{k-1} \cdots b_0. \quad (3)$$

We extend π_k to edges by $\pi_k((u, v)) = (\pi_k(u), \pi_k(v))$.

The merge operation replaces e_1, e_2 with a single edge $e' = (\pi_p(u_1), \pi_p(v_1))$ in the reduced space, where p is the merge position in the current compressed labels.

The graph compression algorithm (Algorithm 2) works as follows. Starting with the original matching M where all edges have n -bit labels, we initialize $M' \leftarrow M$. Each edge $e \in M'$ maintains its own active qubit list \mathcal{A}_e (initially $(0, 1, \dots, n-1)$), weight-reducing list \mathcal{W}_e (initially empty), and original XOR mask μ_e . The algorithm repeatedly searches for pairs of edges that can be merged according to Definition 4. When edges e_1 and e_2 are merged at position p , they are replaced by a single edge $e' = (\pi_p(u_1), \pi_p(v_1))$. The new active qubit list $\mathcal{A}_{e'}$ is obtained by removing the p -th element from \mathcal{A}_{e_1} . If the removed original qubit index corresponds to a bit set in μ_{e_1} (i.e., it was a differing bit in the original edge), then that index is appended to $\mathcal{W}_{e'}$.

The algorithm terminates when no more mergeable pairs exist. The output is a set of compressed edges, where each compressed edge e' has its own $\mathcal{A}_{e'}$ and $\mathcal{W}_{e'}$. Edges that were never merged retain their original n -bit labels. See Sec. III D for an example of the graph compression algorithm.

C. Circuit construction and Trotterization

For circuit construction, each compressed edge $e' = (u', v')$ with metadata $(\mathcal{A}_{e'}, \mathcal{W}_{e'})$ is implemented as a three-stage circuit. Let q_{target} denote the target qubit of the multicontrolled Rx gate, which is one of the bit positions where u' and v' differ in the compressed representation; the corresponding original qubit index is $\mathcal{A}_{e'}[q_{\text{target}}]$.

The first stage applies CX gates to transform the computational basis so that the original edge (which may have Hamming distance greater than one) becomes Hamming distance one in the transformed basis. Specifically, for each original qubit index $w \in \mathcal{W}_{e'}$, a CX gate is applied with control on original qubit $\mathcal{A}_{e'}[q_{\text{target}}]$ and target on original qubit w .

The second stage applies the multicontrolled Rx($2t$) gate that implements the edge evolution. The target of this gate is original qubit $\mathcal{A}_{e'}[q_{\text{target}}]$, corresponding to a differing bit in the compressed edge. The control qubits are all other qubits in $\mathcal{A}_{e'}$, namely $\{\mathcal{A}_{e'}[p] : p \neq q_{\text{target}}\}$, with control values determined by the common bits of u' and v' . For fully compressed edges where the compressed labels are single-qubit strings, this reduces to a simple Rx($2t$) gate with no controls.

Algorithm 2: Iterative Graph Compression

```

Input: Matching  $M \subseteq \{0, 1\}^n \times \{0, 1\}^n$ 
Output: Set of tuples  $(e', \mathcal{A}_{e'}, \mathcal{W}_{e'}, \mu_{e'})$  for each edge
1 for each edge  $e = (u, v) \in M$  do
2    $\mathcal{A}_e \leftarrow (0, 1, \dots, n-1)$ ;           // ordered list
3    $\mathcal{W}_e \leftarrow ()$ ;                      // empty list
4    $\mu_e \leftarrow u \oplus v$ ;                  // original XOR mask
5 end
6  $M' \leftarrow M$ ;
7 repeat
8   for each pair  $e_1, e_2 \in M'$  with  $\mu_{e_1} = \mu_{e_2}$  do
9      $\mathcal{A}_{e_1} = \mathcal{A}_{e_2}$ ,  $\mathcal{W}_{e_1} = \mathcal{W}_{e_2}$  do
10    for  $p = 0$  to  $|\mathcal{A}_{e_1}| - 1$  do
11      if  $(u_1 \oplus u_2) = (v_1 \oplus v_2) = 2^p$  or
12         $(u_1 \oplus v_2) = (v_1 \oplus u_2) = 2^p$  then
13           $e' \leftarrow (\pi_p(u_1), \pi_p(v_1))$ ;
14           $\mathcal{A}_{e'} \leftarrow \mathcal{A}_{e_1}$  with element at position  $p$ 
15            removed;
16           $\mathcal{W}_{e'} \leftarrow \mathcal{W}_{e_1}$ ;
17           $k \leftarrow \mathcal{A}_{e_1}[p]$ ; // original qubit index
18          if bit  $k$  is set in  $\mu_{e_1}$  then
19            | append  $k$  to  $\mathcal{W}_{e'}$ 
20          end
21           $\mu_{e'} \leftarrow \mu_{e_1}$ ;
22           $M' \leftarrow (M' \setminus \{e_1, e_2\}) \cup \{e'\}$ ;
23          break;
24        end
25      end
26    end
27  end
28 until no merge performed;
29 return  $\{(e', \mathcal{A}_{e'}, \mathcal{W}_{e'}, \mu_{e'}) : e' \in M'\}$ ;

```

The third stage reverses the basis transformation by applying the same CX gates as in the first stage. Edges that are not compressed are implemented directly using the single-edge circuit construction from [21], which follows the same pattern: X gates to transform to the all-ones basis, CX gates for Hamming distance reduction, a multicontrolled Rx gate, and the inverse transformations.

After constructing circuits for all matchings (that may or may not contain compressed edges), we approximate the full CTQW evolution via Trotterization. For matchings $\{M_j\}_{j=1}^m$ decomposing graph G , we have $A_G = \sum_{j=1}^m A_{M_j}$.

D. Example

Let us implement the matching decomposition algorithm on the graph in Fig. 1. The matching algorithm first identifies that edges 00-01 and 10-11 have bit-flip position 0 and no edges have bit-flip position 1. Thus, 00-01 and 10-11 are added to matching M_0 . The remaining two edges 00-11 and 01-10 cannot be added to M_0 since they share vertices with edges already contained in M_0 . Thus we place them into a second matching called M_1 .

After assigning each edge to a matching, we apply the

iterative graph compression techniques to each matching. The edges of M_0 differ only in qubit 0, compressing to a single edge $(0, 1)$ with $\mathcal{A} = \{0\}$ and $\mathcal{W} = \{\}$. For M_1 , both edges $(00, 11)$ and $(01, 10)$ have Hamming distance 2, differing in both qubits. Iterative compression eliminates qubit 0 (which varies across the matching), yielding a compressed edge $(0, 1)$ with $\mathcal{A} = \{1\}$ and $\mathcal{W} = \{0\}$. The non-empty \mathcal{W} reflects that qubit 0 contributed to the Hamming distance within each original edge.

Finally, we construct the circuits for each compressed matching. The compressed edge for M_0 requires only a single $\text{Rx}(2t)$ gate on qubit 0. For M_1 , the non-empty weight-reducing set $\mathcal{W} = \{0\}$ requires additional CX gates: we first apply a CX gate with control on qubit 1 (the target of the Rx gate) and target on qubit 0, then apply $\text{Rx}(2t)$ on qubit 1, and finally reverse the CX gate. The complete circuit for one Trotter step is shown in Fig. 2; multiple Trotter steps are implemented by repeating this circuit sequence with appropriately scaled rotation angles.

IV. RESULTS

In this section, we first calculate the operator norm difference between CTQW unitaries and the unitary resulting from Trotterization using our matching decomposition algorithm on a test set of graphs and compare it to the operator norm difference between the CTQW unitary and Trotterization using Pauli decomposition to show that both methods converge at similar rates. We perform Pauli decomposition by iterating through all 4^n Pauli strings and calculating the coefficient $c_P = \text{Tr}(P^\dagger A)/2^n$ for each Pauli operator P and the graph adjacency matrix A . Note that this is a simple reference implementation and the benchmarks are the properties of the compiled circuit and not coefficient finding. Non-zero terms are collected into Qiskit's `SparsePauliOp` [49], and the circuit is constructed using Qiskit's `PauliEvolutionGate` [61] for each Trotter step. Code for our matching algorithm and Pauli decomposition can be found at the linked repository below. We then calculate the CX gate count and circuit depth that matching decomposition requires to simulate CTQWs on test sets of graphs with between 8 and 128 vertices and compare it to the CX gate count and circuit depth that Pauli decomposition requires to simulate the same graphs. Finally, we analytically analyze graphs that have a commuting matching decomposition. Note that this does not imply that our matching decomposition algorithm will find this matching.

We use first-order Trotterization throughout this work for simplicity. All circuits are constructed using Qiskit 1.2.2, full connectivity, basis of CX and U_3 (an arbitrary single qubit unitary), and optimized at level 3.

A. Operator difference 2-norm

We study the error induced by using matching decomposition as a basis for Trotterization, $\|e^{-iAt} - U_{\text{matching}}\|_2$, and compare it to the error induced by using Pauli decomposition in Trotterization by computing $\|e^{-iAt} - U_{\text{Pauli}}\|_2$, where A is the graph adjacency matrix and U_{matching} (U_{Pauli}) is the operator resulting from using Trotterization with matching (Pauli) decomposition. Figure 3 shows the average 2-norm operator difference for a set of 80 randomly generated sparse connected 8-vertex graphs with mean values over all graphs and shaded ± 1 standard deviation regions. Convergence plots for 200 randomly generated connected graphs on both 16- and 32-vertices, 74 randomly generated disconnected 8-vertex graphs, and 200 randomly generated disconnected graphs on both 16- and 32-vertices can be found in Appendix A.

At $t = 1.0$ and $N = 100$, connected graphs achieve mean errors of $9.1\text{--}9.5 \times 10^{-3}$ with $\sim 15\%$ relative standard deviation across graph sizes. Disconnected graphs show lower mean errors ($6.1\text{--}6.7 \times 10^{-3}$) due to fewer edges and thus fewer non-commuting terms, but higher relative variance ($\sim 30\%$). Some disconnected graphs achieve machine-precision errors when all matchings commute. The matching and Pauli decompositions achieve nearly identical accuracy across all cases, confirming that matching decomposition provides a valid basis for Trotterization.

B. CX gate count and circuit depth

Next, we compare the gate counts for one iteration of Trotterization using the matching decomposition and Pauli decomposition on two datasets, implemented using Qiskit's transpiler [62] at optimization level 3 to optimize the resulting circuits. Circuit depth is the number of layers of gates executed in parallel. The first dataset consists of connected graphs that are generated as Hamiltonian paths on $N = 2^n$ vertices for $n \in \{3, 4, 5, 6, 7\}$ that visit vertices labeled in numerical order $0 \dots 0 \rightarrow 0 \dots 01 \rightarrow 0 \dots 010 \rightarrow \dots \rightarrow 1 \dots 1$ or slight modifications of Hamiltonian paths. See the repository linked at the end of the paper for code that generates these graphs and details on the modifications to the Hamiltonian paths. These graphs have $O(N)$ edges and have a characteristic Hamming weight distribution: for all $i \leq n$, approximately $\frac{N}{2^i} = \frac{2^n}{2^i}$ edges lie in H_i where $H_k = \{uv \in E : d_H(u, v) = k\}$. The graphs have large diameter, low maximum degree, low edge density, and are frequently bipartite (19–60% of graphs, with smaller graphs more frequently bipartite). Properties of graphs in this dataset are shown in Table I.

The average CX gate counts and circuit depths are shown in Figure 4. For each value of N , we generate 200 graphs that have the above properties and run the matching decomposition and Pauli decomposition algorithms 5 times as both the matching heuristic and Qiskit optimizer

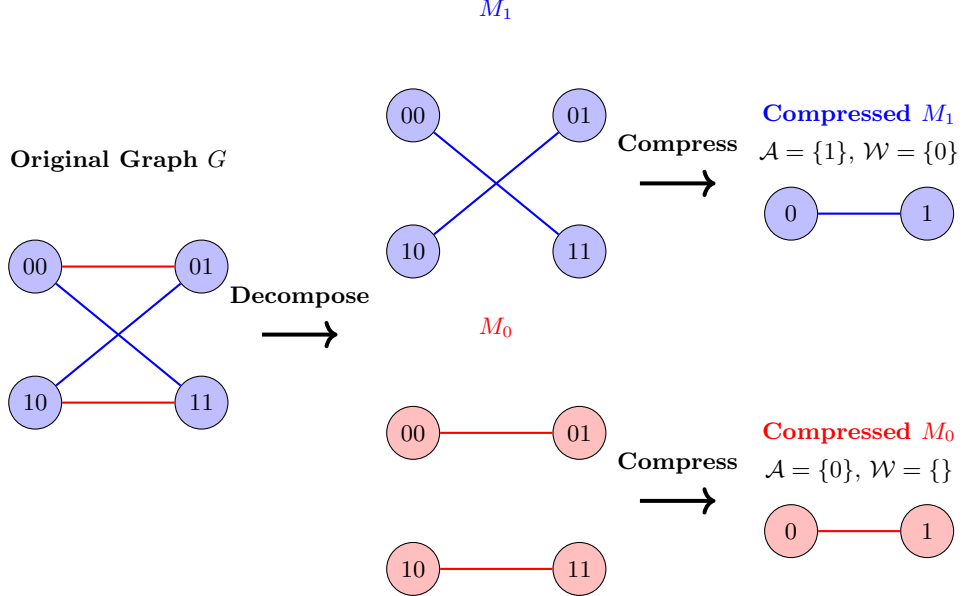


FIG. 1. Matching decomposition and space reduction example. The original 4-vertex graph G with edges $\{(00, 01), (10, 11), (00, 10), (01, 10)\}$ decomposes into two matchings. M_0 (red) contains Hamming distance 1 edges $\{(00, 01), (10, 11)\}$ which differ only in qubit 0, compressing to a single edge $(0, 1)$ with active qubits $\mathcal{A} = \{0\}$ and weight-reducing qubits $\mathcal{W} = \{\}$. M_1 (blue) contains Hamming distance 2 edges $\{(00, 10), (01, 10)\}$, compressing to edge $(0, 1)$ with $\mathcal{A} = \{1\}$ and $\mathcal{W} = \{0\}$. The non-empty \mathcal{W} for M_1 indicates that CX gates are required for the basis transformation.

TABLE I. Properties of the connected graph datasets (mean \pm std, averaged over all graphs in each dataset). Bipartite % shows the fraction of graphs that are bipartite. Connected graphs are single-component counting paths with $\sim N$ edges.

Vertices	Edges	Avg Degree	Max Degree	Density	Bipartite %
<i>Connected datasets</i>					
8	8.8 ± 0.4	2.2 ± 0.1	3.3 ± 0.5	0.32 ± 0.01	22%
16	16.7 ± 0.5	2.1 ± 0.1	3.1 ± 0.4	0.14	32%
32	32.8 ± 0.4	2.1 ± 0.03	3.1 ± 0.3	0.07	26%
64	65.2 ± 0.6	2.0 ± 0.02	3.1 ± 0.3	0.03	24%
128	129.6 ± 0.7	2.0 ± 0.01	3.1 ± 0.3	0.02	18%

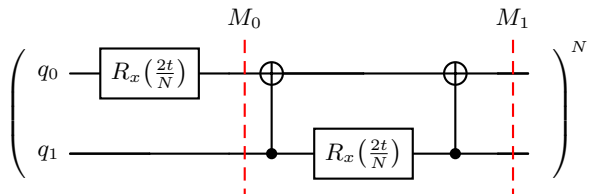


FIG. 2. Trotterized circuit for the example graph with N Trotter steps. The $R_x(2t/N)$ gate on q_0 implements M_0 . The CX- $R_x(2t/N)$ -CX sequence implements M_1 , where the CX gates perform the basis transformation required by $\mathcal{W} = \{0\}$. The entire sequence is repeated N times.

are nondeterministic. On smaller datasets (8 and 16 vertices) the matching decomposition on average requires more CX gates than Pauli decomposition. However, the crossover occurs at 32 vertices: matching decomposition requires 8% fewer CX gates on average, increasing to 34%

fewer at 64 vertices and 43% fewer at 128 vertices. Circuit depth follows a similar pattern: on 8- and 16-vertex graphs, matching decomposition produces deeper circuits than Pauli decomposition, but matching decomposition produces 21% shallower circuits at 32 vertices, 40% shallower circuits at 64 vertices, and 54% shallower circuits at 128 vertices for connected graphs.

The shaded regions in Figure 4 show the standard deviation across graphs, expressed as a coefficient of variation ($CV = \text{std}/\text{mean}$). For connected graphs, matching decomposition exhibits higher relative variance ($CV = 35\text{--}46\%$) compared to Pauli decomposition ($CV = 15\text{--}22\%$), reflecting matching decomposition's sensitivity to graph structure or choice of matching. Interestingly, matchings that consist purely of edges in H_1 (e.g., Gray code paths on hypercubes) consistently require *more* CX gates to implement than Pauli decomposition does—the mixed Hamming structure is essential for reduced CX gate count. Based on these observations, we believe the

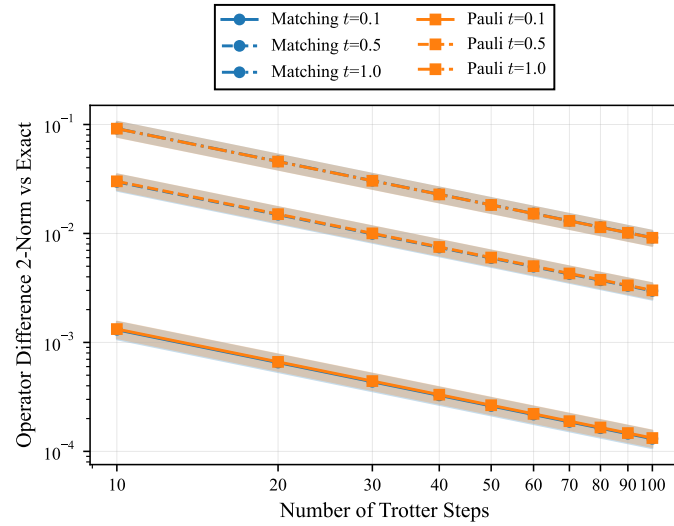


FIG. 3. The 2-norm of the operator difference $\|e^{-iAt} - U_{\text{Trotter}}\|_2$ between the exact CTQW evolution and Trotterized approximations for the 8-vertex connected graph dataset. Lines show mean values over all graphs for matching decomposition (blue, circles) and Pauli decomposition (orange, squares), with shaded regions indicating ± 1 standard deviation. Line styles distinguish evolution times: solid ($t = 0.1$), dashed ($t = 0.5$), and dash-dot ($t = 1.0$). Trotter steps range from $N = 10$ to $N = 100$. Both methods exhibit comparable convergence rates, with errors scaling as $O(t^2/N)$.

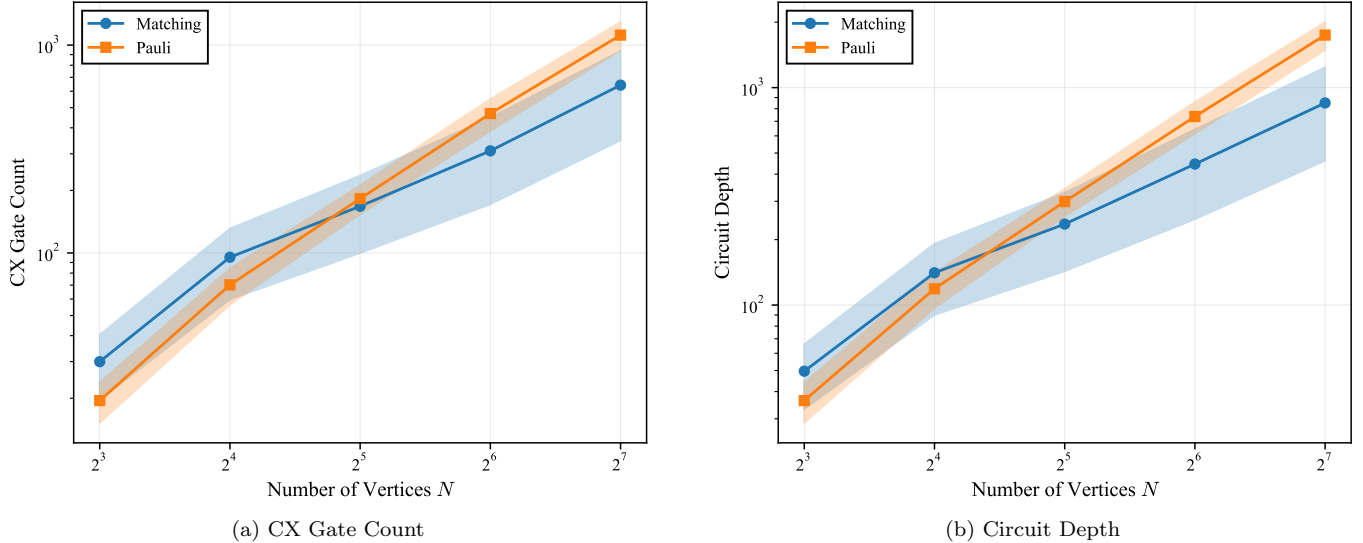


FIG. 4. CX gate counts and circuit depths for the matching and Pauli decompositions on the connected graph datasets. Shaded regions indicate standard deviation across graphs.

CX gate count when simulating CTQWs on graphs using Trotterization with matching decomposition will be lower than the CX gate count when using Trotterization with Pauli decomposition on sparse graphs where there are edges that connect vertices with large Hamming distance, but there is no regular structure to the graph. We believe this because Pauli decomposition of edges that connect vertices with large Hamming distance should require nonlocal terms, and the irregularity ensures that there are few terms in the Pauli decomposition that can be simplified.

The second dataset consists of Erdős-Rényi random graphs generated with the NetworkX `gnp_random_graph(N, p)` function [63] for $N \in \{8, 16, 32, 64, 128\}$ nodes and $p = .01$ probability of an edge existing. For each N , we generate 100 random graphs.

Figure 5 shows the CX gate count and circuit depth for `gnp_random_graph($N, .01$)`. The CX gate count (Fig. 5a) for matching decomposition is less than Pauli decomposition when $N \geq 32$, achieving reductions of 25% at $N = 32$, 33% at $N = 64$, and 31% at $N = 128$. The cir-

cuit depth (Fig. 5b) shows similar trends, with matching decomposition producing 37%, 41%, and 49% shallower circuits at $N = 32, 64$, and 128 respectively. The shaded regions indicate standard deviation across graphs. For this dataset, the CV for the matching decomposition CX counts decreases from 29% at 32 vertices to 10% at 128 vertices, indicating increasingly predictable performance for larger N .

The Erdős-Rényi datasets indicate that sparseness of a graph G may be a property that indicates if matching decomposition requires fewer CX gates than Pauli decomposition when simulating G in the circuit model. However, the connected dataset indicates that matching decomposition can require fewer CX gates than Pauli decomposition on denser graphs if the denser graphs satisfy certain properties such as distribution of edges with particular Hamming weights. Interestingly, the connected datasets achieve larger CX reductions than Erdős-Rényi graphs but exhibit higher variance. The connected graphs were designed based on the hypothesis that Hamming weight distribution is the primary structural factor determining matching decomposition performance. However, the persistently high variance suggests that Hamming weight distribution alone does not fully explain performance—other structural properties likely also play significant roles. Future work could investigate these additional structural factors to develop graph generation methods that achieve both large CX reductions and low variance.

C. Commutativity

We now provide a class of simple graphs where 1.) there exists a matching decomposition such that the matchings commute and 2.) the standard Pauli decomposition has terms that do not pairwise commute. Let us define a *non-commuting Pauli decomposition* to be the standard Pauli decomposition that has terms that do not all pairwise commute and let us define *commuting matching decomposition* of a subgraph G' as a decomposition of the edges of G' into matchings such that the adjacency matrix of each matching of G' pairwise commute. We emphasize that the existence of a commuting matching decomposition does not imply that our matching decomposition algorithm will find this matching.

First, let us consider when the adjacency matrices of two arbitrary subgraphs commute.

Lemma 1. *Let $G = (V, E)$ be a simple, undirected graph. Two arbitrary subgraphs $G' = (V, E')$ and $G'' = (V, E'')$ of G commute if and only if for any $(u, v) \in V \times V$,*

$$|\{w \in V \mid (u, w) \in E' \text{ and } (w, v) \in E''\}| = |\{w \in V \mid (u, w) \in E'' \text{ and } (w, v) \in E'\}|$$

Proof. Let A' be the adjacency matrix of G' and A'' the adjacency matrix of G'' . Consider matrix element $[u, v]$

of their product:

$$(A' A'')_{uv} = \sum_{w \in V} A'_{uw} A''_{vw}$$

Each summand $A'_{uw} A''_{vw}$ is equal to 1 when $(u, w) \in E'$ and $(w, v) \in E''$, therefore $(A' A'')_{uv}$ counts the number of length-2 paths where the first edge belongs to E' and the second edge belongs to E'' . $(A'' A')_{uv}$ does the same except the first edge belongs to E'' and the second to E' . Therefore, the subgraphs commute if and only if the number of these paths is the same regardless of order of subgraphs. \square

Less formally, Lemma 1 requires that the number of length-2 paths between arbitrary 2 vertices of type (E', E'') (i.e. where the first edge belongs to E' and the second edge belongs to E'') is the same as the number of paths of type (E'', E') between the same vertices, so the paths are balanced.

In the particular case when the subgraphs are matchings, Lemma 1 is reduced to the following lemma.

Lemma 2. *Two matchings $G' = (V, E')$ and $G'' = (V, E'')$ of a graph G commute if and only if each connected component of their union is either an isolated vertex (K_1), single edge (K_2) or a 4-cycle (C_4).*

Proof. The degree of each vertex in a matching is either 0 or 1. Therefore, in a union of 2 matchings the degree of each vertex is ≤ 2 . Therefore, structurally, the union of 2 matchings consists of isolated vertices, and paths or cycles where edges alternate between the two matchings. Isolated vertices and single edges do not change the number of length-2 paths in the graph, so they do not affect commutativity according to Lemma 1. If there is a path that consists of more than 1 edge, then we can always consider its first and third vertices. There is only 1 path of length-2 between these vertices, therefore the matchings would not commute according to Lemma 1. In case of a cycle, if the length of the cycle is more than 4, then we can apply the same argument as for a path to conclude that these matchings do not commute. The only case when they still commute is if the cycle length is exactly 4, in which case the number of length-2 paths of each type between any 2 vertices of the cycle is balanced (either 0 or 1). \square

A similar result has also been proven for perfect matchings in [64].

Our next result shows that a commuting matching remains commuting under relabeling of vertices. We emphasize that we are using a standard Pauli decomposition pipeline and that there may exist more advanced Pauli decomposition techniques that allow one to exactly implement the below unitaries without using Trotterization.

Lemma 3. *A commuting matching decomposition of the adjacency matrix A of a graph is still commuting after a relabeling of the vertices.*

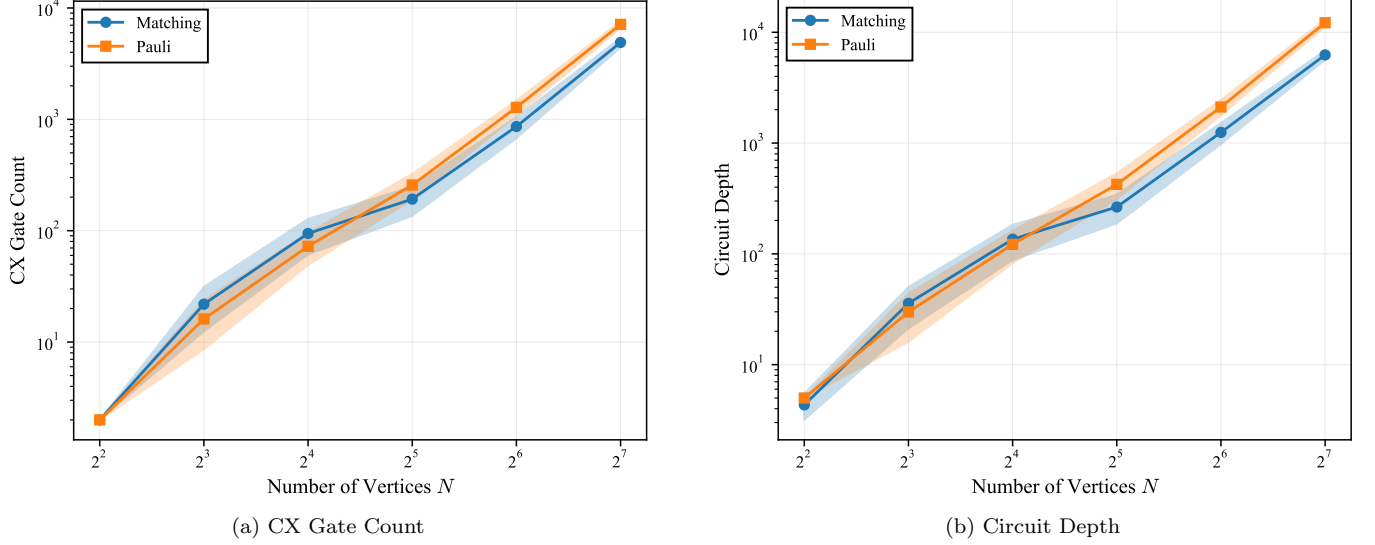


FIG. 5. CX gate counts and circuit depth for matching decomposition (blue) and Pauli decomposition (orange) on Erdős-Rényi random graphs with $p = 0.01$. Matching decomposition requires 25%, 33%, and 31% fewer CX gates at $N = 32, 64$, and 128 respectively, and produces 37%, 41%, and 49% shallower circuits.

Proof. A relabeling of vertices is a bijection $f(x) : \{0, 1\}^n \rightarrow \{0, 1\}^n$. Since it is a bijection of the standard basis states, $f(x)$ corresponds to a permutation unitary transformation U_f of the adjacency matrix. Let $M = \{M_k\}$ be a commuting matching decomposition. Then $A = \sum_k A_{M_k}$, where A_{M_k} is the adjacency matrix of M_k . Let $A' = U_f A U_f^\dagger$. First note that A' is an adjacency matrix since it is still 0-1 valued and is symmetric since $f(x)$ is a bijection. Furthermore, $[U_f A_{M_k} U_f^\dagger, U_f A_{M_l} U_f^\dagger] = 0$ for all $k \neq l$. Then $M' = \{f(M_k)\}$ is a commuting matching decomposition of A' . \square

Consider the adjacency matrix $A = \sum_i^n X_i$. This corresponds to the discrete hypercube graph Q_n , which has 2^n vertices labeled by all unique n -bitstrings and edges connecting vertices that are Hamming distance one apart.

Lemma 4. Consider the discrete hypercube with eight vertices, which has adjacency matrix $A = \sum_{i=1}^3 X_i$. Let $f_n(x) = 3x \bmod (2^n)$. The permutation $f_3(x)$ results in an adjacency matrix A' with a commuting matching decomposition and non-commuting Pauli decomposition (contains IXI and IYY).

Proof. For the initial adjacency matrix A , there exists a matching decomposition $M = \sum_{j=1}^n M_j$, where each matching M_j corresponds to all edges that differ in exactly bit j . From Lemma 1, all M_j are pairwise commuting since their edges form 4-cycles, so M is a commuting matching decomposition. From Lemma 3, $M' = f_3(M)$ is a commuting matching decomposition for A' .

From direct calculation,

$$U_f = \begin{pmatrix} 1 & 0 & 0 & 0 & 0 & 0 & 0 & 0 \\ 0 & 0 & 0 & 1 & 0 & 0 & 0 & 0 \\ 0 & 0 & 0 & 0 & 0 & 0 & 1 & 0 \\ 0 & 1 & 0 & 0 & 0 & 0 & 0 & 0 \\ 0 & 0 & 0 & 0 & 1 & 0 & 0 & 0 \\ 0 & 0 & 0 & 0 & 0 & 0 & 0 & 1 \\ 0 & 0 & 1 & 0 & 0 & 0 & 0 & 0 \\ 0 & 0 & 0 & 0 & 0 & 1 & 0 & 0 \end{pmatrix} \quad (4)$$

and

$$A' = \begin{pmatrix} 0 & 0 & 0 & 1 & 1 & 0 & 1 & 0 \\ 0 & 0 & 0 & 1 & 0 & 1 & 1 & 0 \\ 0 & 0 & 0 & 0 & 1 & 1 & 1 & 0 \\ 1 & 1 & 0 & 0 & 0 & 0 & 0 & 1 \\ 1 & 0 & 1 & 0 & 0 & 0 & 0 & 1 \\ 0 & 1 & 1 & 0 & 0 & 0 & 0 & 1 \\ 1 & 1 & 1 & 0 & 0 & 0 & 0 & 0 \\ 0 & 0 & 0 & 1 & 1 & 1 & 0 & 0 \end{pmatrix}. \quad (5)$$

Then $\text{tr}(IXIA') = 4$ and $\text{tr}(IYYA') = -4$. Thus, the Pauli decomposition of A' contains IXI and IYY which anti-commute. \square

We can easily extend this to an infinite family of hypercubes.

Corollary 1 (Family of hypercubes). Let $A_n = \sum_i^n X_i$ be the adjacency matrix of Q_n . Index the labels of the vertices as $b_{n-1}b_{n-2} \dots b_0$. Then the adjacency matrix A'_n associated with the permutation relabeling

$$g_i(b_{n-1}b_{n-2} \dots b_0) = b_{n-1} \dots f_3(b_{i+2}b_{i+1}b_i) \dots b_0 \quad (6)$$

for any i between 0 and $n-3$ has a commuting matching decomposition and non-commuting Pauli decomposition.

Proof. A' has a commuting matching decomposition by Lemma 1 and Lemma 3. Function g_i induces a unitary $U = I^{\otimes(n-i-3)} \otimes U_f \otimes I^{\otimes i}$. Next, $A' = UAU^\dagger = \sum_j^n UX_jU^\dagger$. This unitary only acts non-trivially on qubits $i, i+1$, and $i+2$ by definition of Eq. (6). From Lemma 4, we know that X_{i+1} and $Y_{i+2}Y_{i+1}$ are terms in the Pauli decomposition of A' , which anti-commute. \square

The previous results hold for an infinite collection of graphs with specific structure. The remainder of this section will provide results for graphs with less rigid structure. If a collection of matchings $\{M_j\}_{j=1}^k$ satisfies

$$A_G = A_{M_1} + \dots + A_{M_k}$$

where A_G is the adjacency matrix of some graph G , and A_{M_j} is the adjacency matrix of matching j , $e^{-iA_G t} = e^{-i\sum_{j=1}^k A_{M_j} t}$. If all A_{M_j} pairwise commute, then $e^{-i\sum_{j=1}^k A_{M_j} t} = \prod_{j=1}^k e^{-iA_{M_j} t}$. Thus, a CTQW on graph G is exactly implementable using matching decompositions if and only if the adjacency matrices of all matchings in $\{M_j\}_{j=1}^k$ pairwise commute. For non-commuting operators we have the approximation

$$(e^{-i\frac{t}{N}A_{M_1}}e^{-i\frac{t}{N}A_{M_2}}\dots e^{-i\frac{t}{N}A_{M_k}})^N = e^{-itA_G} + O(t^2/N)$$

with the error bound depending on the commutator norms $\|[A_{M_i}, A_{M_j}]\|$.

The authors of [64] also remark:

Remark 1. [64] *By the previous lemma, we conclude that for a k -regular graph G , G is decomposable into commuting perfect matchings if and only if G has a 1-factorization such that the union of any two distinct perfect matchings in the 1-factorization is a disjoint union of copies of C_4 .*

Here, a 1-factorization of a k -regular graph G is defined as a partition of the edges into k perfect matchings. It is known that discrete hypercubes, Q_n , satisfy this property [65, 66]. Q_n is a graph on 2^n vertices such that each vertex has an n bitstring label, and two vertices u and v are adjacent if and only if the Hamming distance between their labels is exactly 1. Interestingly, Q_n is a type of circulant graph, the walks on which are known to be exactly implementable in the circuit model [32]. However, this approach requires the Quantum Fourier Transform (QFT) to change the computational basis, along with multi-controlled rotation gates. The matching decomposition approach, in general, appears to require fewer controlled gates to implement walks on Q_n than the QFT approach.

However, it is not clear which graphs satisfy this property in general. One result from [67] shows that the result holds for complete bipartite graphs if each partition has 2^n vertices for some n .

Lemma 5. [67] *Let n be a natural number. The graph $K_{n,n}$ is decomposable into commuting perfect matchings if and only if n is a power of 2.*

Thus, a characterization of the graphs that satisfy Lemma ?? will also provide a set of graphs G such that the CTQWs on G can be exactly implemented using matching decomposition.

V. DISCUSSION

In this work, we develop a new matching heuristic that requires only polynomial complexity classical overhead and can be used as a basis for Trotterization when approximating CTQWs in the circuit model. We use the adjacency matrices of these matchings as Hamiltonians in a Trotterization of $e^{-tA_G t}$ for graphs G with adjacency matrix A_G and compare these methods to Trotterization with Pauli decomposition [49]. While both matching decomposition and Pauli decomposition have similar quantum gate complexity, matching decomposition achieves lower CX gate counts when used to simulate CTQWs on sparse graphs, as demonstrated in our experiments.

We first find that the 2-norm operator difference between the matching decomposition and the CTQW evolution on sets of 8-, 16-, and 32-vertex graphs is comparable to the 2-norm operator difference between Pauli decomposition and the CTQW evolution. We also simulate CTQWs on sets of connected graphs with between 8 and 128 vertices, as well as Erdős-Rényi graphs with between 8 and 128 vertices with $p = .01$, and compare the gate counts of the matching decomposition to the gate counts for Pauli decomposition when implemented with Qiskit using circuit optimization level 3 on the same datasets. We find that the matching decomposition requires approximately 34%, 42%, and 45% fewer CX gates than Pauli decomposition respectively on the connected 32-, 64-, and 128-vertex graphs when implementing matching decomposition.

While these studies give evidence that matching decomposition can efficiently simulate CTQW Hamiltonian evolution, there are still several open research directions. First, more precise bounds for the CX gate scaling of these approaches would validate the utility of this approach for near-term quantum devices. Second, previous works show that the order of graph matching techniques for state preparation can greatly impact CX gate count [21], so developing heuristics for ordering the matchings to be used in Trotterization can further decrease the gate count. Similarly, randomizing the gates based on the weight of terms in the Hamiltonian can lead to shallower circuits [68].

Third, a better characterization of when matching decomposition requires fewer gates and shorter circuits than Pauli decomposition would be useful for simulating CTQW Hamiltonian evolution in the circuit model. Fourth, CTQWs are well-known for finding marked nodes in a graph. Can the matchings approaches be used to find marked vertices with high probability in shorter time than the full CTQW Hamiltonian evolution can find them? Fifth, it is worth noting that the labels of the

nodes may impact circuit depth, thus finding permutation unitaries that reduce gate count further may be useful [69]. Finally, while matchings are a natural method for decomposing graphs and walks on them are easily implementable in the circuit model, it would be interesting to study if there are other useful graph structures that can be implemented exactly in the circuit model.

AUTHOR CONTRIBUTIONS

MA developed the CTQW graph compression technique, wrote code, and gathered data. DD debugged errors and wrote code to analytically verify unitary equivalences. IG wrote the proof of Lemma 1. AG wrote code, found exact examples, and developed the theoretical idea on the weight-reducing qubits in the edge compression. ZHS suggested the experiments to test the algorithm and secured funding. RH developed the graph matching decomposition and secured funding. All authors wrote, read, edited, and approved the final manuscript.

ACKNOWLEDGMENTS

M. Atallah, I. Gaidai, and R. Herrman acknowledge DE-SC0024290. D. Dilley, A. Gonzales, and Z. Saleem acknowledge DOE-145-SE-14055-CTQW-FY23. The funder played no role in study design, data collection, analysis and interpretation of data, or the writing of this manuscript.

COMPETING INTERESTS

All authors declare no financial or non-financial competing interests.

CODE AND DATA AVAILABILITY

The code and data for this research can be found at <https://github.com/Mostafa-Atallah2020/dyn-CTQW>.

The submitted manuscript has been created by UChicago Argonne, LLC, Operator of Argonne National Laboratory (“Argonne”). Argonne, a U.S. Department of Energy Office of Science laboratory, is operated under Contract No. DE-AC02-06CH11357. The U.S. Government retains for itself, and others acting on its behalf, a paid-up nonexclusive, irrevocable worldwide license in said article to reproduce, prepare derivative works, distribute copies to the public, and perform publicly and display publicly, by or on behalf of the Government. The Department of Energy will provide public access to these results of federally sponsored research in accordance with the DOE Public Access Plan. <http://energy.gov/downloads/doe-public-access-plan>.

REFERENCES

- [1] Guang Hao Low and Nathan Wiebe. Hamiltonian simulation in the interaction picture. *arXiv preprint arXiv:1805.00675*, 2018.
- [2] Guang Hao Low and Isaac L Chuang. Optimal hamiltonian simulation by quantum signal processing. *Physical review letters*, 118(1):010501, 2017.
- [3] Dominic W Berry and Andrew M Childs. Black-box hamiltonian simulation and unitary implementation. *arXiv preprint arXiv:0910.4157*, 2009.
- [4] Rolando D Somma, Robbie King, Robin Kothari, Thomas E O’Brien, and Ryan Babbush. Shadow hamiltonian simulation. *Nature Communications*, 16(1):2690, 2025.
- [5] Shantanav Chakraborty, András Gilyén, and Stacey Jeffery. The power of block-encoded matrix powers: improved regression techniques via faster hamiltonian simulation. *arXiv preprint arXiv:1804.01973*, 2018.
- [6] Dominic W Berry, Andrew M Childs, and Robin Kothari. Hamiltonian simulation with nearly optimal dependence on all parameters. In *2015 IEEE 56th annual symposium on foundations of computer science*, pages 792–809. IEEE, 2015.
- [7] Xiaogang Qiang, Thomas Loke, Ashley Montanaro, Kanin Aungskunsiri, Xiaoqi Zhou, Jeremy L O’Brien, Jingbo B Wang, and Jonathan CF Matthews. Efficient quantum walk on a quantum processor. *Nature communications*, 7(1):11511, 2016.
- [8] Andrew M Childs. Universal computation by quantum walk. *Physical review letters*, 102(18):180501, 2009.
- [9] Andrew M Childs and Jeffrey Goldstone. Spatial search by quantum walk. *Physical Review A*, 70(2):022314, 2004.
- [10] Rebekah Herrman and Travis S Humble. Continuous-time quantum walks on dynamic graphs. *Physical Review A*, 100(1):012306, 2019.
- [11] Shantanav Chakraborty, Leonardo Novo, and Jérémie Roland. Finding a marked node on any graph via continuous-time quantum walks. *Physical Review A*, 102(2):022227, 2020.
- [12] Tomo Osada, Bruno Coutinho, Yasser Omar, Kaoru Sanaka, William J Munro, and Kae Nemoto. Continuous-time quantum-walk spatial search on the Bollobás scale-free network. *Physical Review A*, 101(2):022310, 2020.
- [13] Simon Apers, Shantanav Chakraborty, Leonardo Novo,

and Jérémie Roland. Quadratic speedup for spatial search by continuous-time quantum walk. *Physical review letters*, 129(16):160502, 2022.

[14] Hajime Tanaka, Mohamed Sabri, and Renato Portugal. Spatial search on johnson graphs by continuous-time quantum walk. *Quantum Information Processing*, 21(2):74, 2022.

[15] Mark Goldsmith, Harto Saarinen, Guillermo García-Pérez, Joonas Malmi, Matteo AC Rossi, and Sabrina Maniscalco. Link prediction with continuous-time classical and quantum walks. *Entropy*, 25(5):730, 2023.

[16] João P Moutinho, André Melo, Bruno Coutinho, István A Kovács, and Yasser Omar. Quantum link prediction in complex networks. *Physical Review A*, 107(3):032605, 2023.

[17] Andreas Schreiber, Aurél Gábris, Peter P Rohde, Kaisa Laiho, Martin Štefaňák, Václav Potoček, Craig Hamilton, Igor Jex, and Christine Silberhorn. A 2d quantum walk simulation of two-particle dynamics. *Science*, 336(6077):55–58, 2012.

[18] Samuel Marsh and Jingbo B Wang. Combinatorial optimization via highly efficient quantum walks. *Physical Review Research*, 2(2):023302, 2020.

[19] Nicholas Slate, Edric Matwiejew, Samuel Marsh, and Jingbo B Wang. Quantum walk-based portfolio optimisation. *Quantum*, 5:513, 2021.

[20] Edric Matwiejew and Jingbo B Wang. Quantum walk informed variational algorithm design. *arXiv preprint arXiv:2406.11620*, 2024.

[21] Alvin Gonzales, Rebekah Herrman, Colin Campbell, Igor Gaidai, Ji Liu, Teague Tomesh, and Zain H Saleem. Efficient sparse state preparation via quantum walks. *npj Quantum Information*, 11(1):143, 2025.

[22] Mario D’Acunto. Protein-dna target search relies on quantum walk. *Biosystems*, 201:104340, 2021.

[23] Diego Santiago-Alarcon, Horacio Tapia-McClung, Sergio Lerma-Hernández, and Salvador E Venegas-Andraca. Quantum aspects of evolution: a contribution towards evolutionary explorations of genotype networks via quantum walks. *Journal of the Royal Society Interface*, 17(172):20200567, 2020.

[24] Kunkun Wang, Yuhao Shi, Lei Xiao, Jingbo Wang, Yogen N Joglekar, and Peng Xue. Experimental realization of continuous-time quantum walks on directed graphs and their application in pagerank. *Optica*, 7(11):1524–1530, 2020.

[25] Yang Wang, Shichuan Xue, Junjie Wu, and Ping Xu. Continuous-time quantum walk based centrality testing on weighted graphs. *Scientific Reports*, 12(1):6001, 2022.

[26] Amit Rai, Girish Saran Agarwal, and Jacques HH Perk. Transport and quantum walk of nonclassical light in coupled waveguides. *Physical Review A—Atomic, Molecular, and Optical Physics*, 78(4):042304, 2008.

[27] Hagai B Perets, Yoav Lahini, Francesca Pozzi, Marc Sorel, Roberto Morandotti, and Yaron Silberberg. Realization of quantum walks with negligible decoherence in waveguide lattices. *Physical review letters*, 100(17):170506, 2008.

[28] Robert J Chapman, Matteo Santandrea, Zixin Huang, Giacomo Corrielli, Andrea Crespi, Man-Hong Yung, Roberto Osellame, and Alberto Peruzzo. Experimental perfect state transfer of an entangled photonic qubit. *Nature communications*, 7(1):11339, 2016.

[29] Hao Tang, Xiao-Feng Lin, Zhen Feng, Jing-Yuan Chen, Jun Gao, Ke Sun, Chao-Yue Wang, Peng-Cheng Lai, Xiao-Yun Xu, Yao Wang, et al. Experimental two-dimensional quantum walk on a photonic chip. *Science advances*, 4(5):eaat3174, 2018.

[30] Renato Portugal and Jalil Khatibi Moqadam. Implementation of continuous-time quantum walks on quantum computers. *arXiv preprint arXiv:2212.08889*, 2022.

[31] Anjishnu Adhikari, Bikash K Behera, and Prasanta K Panigrahi. Circuit design for continuous time quantum walks on cycle graph and its experimental demonstration in ibm quantum computer.

[32] T Loke and Jingbo B Wang. Efficient quantum circuits for continuous-time quantum walks on composite graphs. *Journal of Physics A: Mathematical and Theoretical*, 50(5):055303, 2017.

[33] Dengke Qu, Samuel Marsh, Kunkun Wang, Lei Xiao, Jingbo Wang, and Peng Xue. Deterministic search on star graphs via quantum walks. *Physical review letters*, 128(5):050501, 2022.

[34] BL Douglas and JB Wang. Efficient quantum circuit implementation of quantum walks. *Physical Review A—Atomic, Molecular, and Optical Physics*, 79(5):052335, 2009.

[35] Edward Farhi and Sam Gutmann. Quantum computation and decision trees. *Physical Review A*, 58(2):915, 1998.

[36] Sabyasachi Chakraborty, Rohit Sarma Sarkar, Sonjoy Majumder, and Rohit Kishan Ray. Continuous-time quantum walk on a random graph using quantum circuits. *arXiv preprint arXiv:2510.14905*, 2025.

[37] Thomas G Wong. Isolated vertices in continuous-time quantum walks on dynamic graphs. *Physical Review A*, 100(6):062325, 2019.

[38] Rebekah Herrman and Thomas G Wong. Simplifying continuous-time quantum walks on dynamic graphs. *Quantum Information Processing*, 21(2):54, 2022.

[39] Ibukunoluwa A Adisa and Thomas G Wong. Implementing quantum gates using length-3 dynamic quantum walks. *Physical Review A*, 104(4):042604, 2021.

[40] Rebekah Herrman. Relating the multi-angle quantum approximate optimization algorithm and continuous-time quantum walks on dynamic graphs. *arXiv preprint arXiv:2209.00415*, 2022.

[41] Edward Farhi, Jeffrey Goldstone, and Sam Gutmann. A quantum approximate optimization algorithm. *arXiv preprint arXiv:1411.4028*, 2014.

[42] Sujay Kazi, Martín Larocca, Marco Farinati, Patrick J Coles, M Cerezo, and Robert Zeier. Analyzing the quantum approximate optimization algorithm: ansätze, symmetries, and lie algebras. *PRX Quantum*, 6(4):040345, 2025.

[43] Anthony Wilkie, Igor Gaidai, James Ostrowski, and Rebekah Herrman. Quantum approximate optimization algorithm with random and subgraph phase operators. *Physical Review A*, 110(2):022441, 2024.

[44] Xiumei Zhao, Yongmei Li, Guanghui Li, Yijie Shi, Sujuan Qin, and Fei Gao. The symmetry-based expressive qaoa for the maxcut problem. *Advanced Quantum Technologies*, page 2500199, 2025.

[45] Yuan Shi, Kristin M Beck, Veronika Anneliese Kruse, and Stephen B Libby. Preparing angular momentum eigenstates using engineered quantum walks. *Physical Review A*, 110(6):062214, 2024.

[46] Zhaoyang Chen, Guanzhong Li, and Lvzhou Li. Imple-

mentation of a continuous-time quantum walk on a sparse graph. *Physical Review A*, 110(5), November 2024.

[47] Masuo Suzuki. Generalized trotter's formula and systematic approximants of exponential operators and inner derivations with applications to many-body problems. *Communications in Mathematical Physics*, 51(2):183–190, Jun 1976.

[48] Ji Liu, Alvin Gonzales, Benchen Huang, Zain Hamid Saleem, and Paul Hovland. Quclear: Clifford extraction and absorption for quantum circuit optimization. In *2025 IEEE International Symposium on High Performance Computer Architecture (HPCA)*, pages 158–172. IEEE, 2025.

[49] IBM. Sparsepauliop. https://docs.quantum.ibm.com/api/qiskit/qiskit.quantum_info.SparsePauliOp.

[50] Horst Bunke and Bruno T Messmer. Efficient attributed graph matching and its application to image analysis. In *Image Analysis and Processing: 8th International Conference, ICIAP'95 San Remo, Italy, September 13–15, 1995 Proceedings 8*, pages 44–55. Springer, 1995.

[51] Aaron Smalter, Jun Huan, and Gerald Lushington. Gpm: A graph pattern matching kernel with diffusion for chemical compound classification. In *2008 8th IEEE International Conference on BioInformatics and BioEngineering*, pages 1–6. IEEE, 2008.

[52] Richard M Karp, Umesh V Vazirani, and Vijay V Vazirani. An optimal algorithm for on-line bipartite matching. In *Proceedings of the twenty-second annual ACM symposium on Theory of computing*, pages 352–358, 1990.

[53] Jing Ren, Feng Xia, Xiangtai Chen, Jiaying Liu, Mingliang Hou, Ahsan Shehzad, Nargiz Sultanova, and Xiangjie Kong. Matching algorithms: Fundamentals, applications and challenges. *IEEE Transactions on Emerging Topics in Computational Intelligence*, 5(3):332–350, 2021.

[54] Jack Edmonds. Paths, trees, and flowers. *Canadian Journal of mathematics*, 17:449–467, 1965.

[55] Harold N Gabow. An efficient implementation of edmonds' algorithm for maximum matching on graphs. *Journal of the ACM (JACM)*, 23(2):221–234, 1976.

[56] John E Hopcroft and Richard M Karp. An $n^{5/2}$ algorithm for maximum matchings in bipartite graphs. *SIAM Journal on computing*, 2(4):225–231, 1973.

[57] Silvio Micali and Vijay V Vazirani. An $o(\sqrt{|v||e|})$ algorithm for finding maximum matching in general graphs. In *21st Annual symposium on foundations of computer science (Sfcs 1980)*, pages 17–27. IEEE, 1980.

[58] Norbert Blum. A new approach to maximum matching in general graphs. In *Automata, Languages and Programming: 17th International Colloquium Warwick University, England, July 16–20, 1990 Proceedings 17*, pages 586–597. Springer, 1990.

[59] Harold N Gabow and Robert E Tarjan. Faster scaling algorithms for general graph matching problems. *Journal of the ACM (JACM)*, 38(4):815–853, 1991.

[60] Michel L Lapidus. Generalization of the trotter-lie formula. *Integral Equations and Operator Theory*, 4:366–415, 1981.

[61] IBM. Paulievolutiongate. <https://docs.quantum.ibm.com/api/qiskit/qiskit.circuit.library.PauliEvolutionGate>.

[62] IBM. Qiskit transpiler. <https://docs.quantum.ibm.com/api/qiskit/transpiler>, 2024. Accessed: 2025.

[63] NetworkX Developers. networkx.generators.random_graphs.gnp_random_graph. https://networkx.org/documentation/stable/reference/generated/networkx.generators.random_graphs.gnp_random_graph.html, 2024. Accessed: 2025.

[64] Saieed Akbari and Allen Herman. Commuting decompositions of complete graphs. *Journal of Combinatorial Designs*, 15(2):133–142, 2007.

[65] Natalie C Behague. Semi-perfect 1-factorizations of the hypercube. *Discrete Mathematics*, 342(6):1696–1702, 2019.

[66] PJ Laufer. On strongly hamiltonian complete bipartite graphs. *Ars Combin*, 9:43–46, 1980.

[67] Saieed Akbari, F Moazami, and A Mohammadian. Commutativity of the adjacency matrices of graphs. *Discrete mathematics*, 309(3):595–600, 2009.

[68] Earl Campbell. Random compiler for fast hamiltonian simulation. *Physical review letters*, 123(7):070503, 2019.

[69] Igor Gaidai and Rebekah Herrman. Decomposition of sparse amplitude permutation gates with application to preparation of sparse clustered quantum states. *arXiv preprint arXiv:2504.08705*, 2025.

Appendix A: Operator norm convergence plots

Figures 6 and 7 show the operator 2-norm difference between the exact CTQW Hamiltonian and the matching decomposition and Pauli decomposition approximations. Both methods exhibit comparable convergence rates, with errors scaling as $O(t^2/N)$.

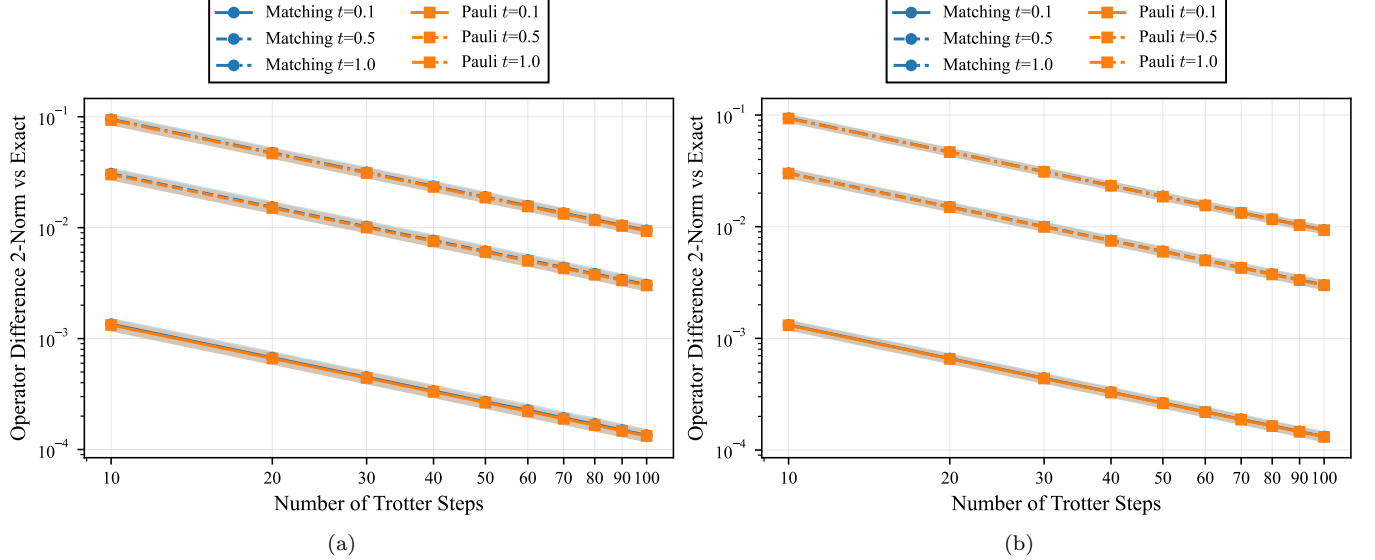


FIG. 6. Operator difference 2-norm $\|e^{-iAt} - U_{\text{Trotter}}\|_2$ between the exact CTQW evolution and Trotterized approximations for sparse connected graphs: (a) 200 graphs on 16 vertices, and (b) 200 graphs on 32 vertices. Lines show mean values over all graphs for matching decomposition (blue, circles) and Pauli decomposition (orange, squares), with shaded regions indicating ± 1 standard deviation. Line styles distinguish evolution times: solid ($t = 0.1$), dashed ($t = 0.5$), and dash-dot ($t = 1.0$). Trotter steps range from $N = 10$ to $N = 100$.

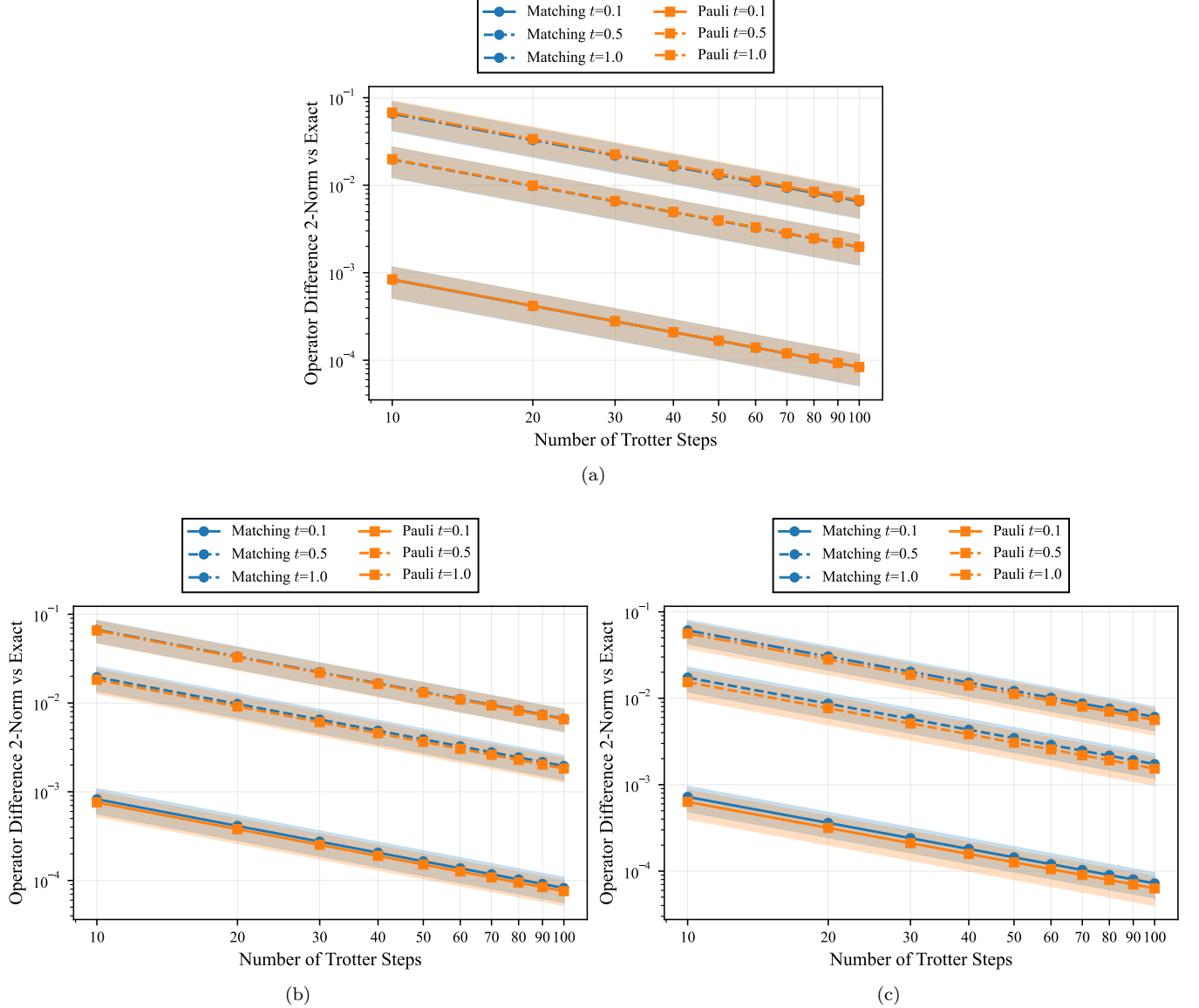


FIG. 7. Operator difference 2-norm $\|e^{-iAt} - U_{\text{Trotter}}\|_2$ between the exact CTQW evolution and Trotterized approximations for sparse disconnected graphs: (a) 74 graphs on 8 vertices, (b) 200 graphs on 16 vertices, and (c) 200 graphs on 32 vertices. Lines show mean values over all graphs for matching decomposition (blue, circles) and Pauli decomposition (orange, squares), with shaded regions indicating ± 1 standard deviation. Line styles distinguish evolution times: solid ($t = 0.1$), dashed ($t = 0.5$), and dash-dot ($t = 1.0$). Trotter steps range from $N = 10$ to $N = 100$.